Environmental Research 195 (2021) 110747

Contents lists available at ScienceDirect

Environmental Research

journal homepage: www.elsevier.com/locate/envres

Superoxide radical enhanced photocatalytic performance of styrene alters its degradation mechanism and intermediate health risk on TiO_2/graphene surface

Jiangyao Chen [a,b], Zilong Zhang [a,b], Weikun Zhu [a,b], Liyun Zhang [a,b], Baocong Zhao [a,b], Yuemeng Ji [a,b], Guiying Li [a,b], Taicheng An [a,b,*]

[a] Guangdong Key Laboratory of Environmental Catalysis and Health Risk Control, Guangdong-Hong Kong-Macao Joint Laboratory for Contaminants Exposure and Health, Institute of Environmental Health and Pollution Control, Guangdong University of Technology, Guangzhou, 510006, China
[b] Guangzhou Key Laboratory of Environmental Catalysis and Pollution Control, Key Laboratory of City Cluster Environmental Safety and Green Development, School of Environmental Science and Engineering, Guangdong University of Technology, Guangzhou, 510006, China

ARTICLE INFO

Keywords:
Graphene coupled semiconductor
Enhanced degradation performance
Promoted superoxide radical
Altered dominant intermediate
Increased health risk

ABSTRACT

Enhancement of reactive oxygen species (ROS) on semiconductor coupled by carbon material promotes photocatalytic performance toward aromatic hydrocarbons, while the contribution to their degradation mechanism and health risk is not well understood. Herein, photocatalytic degradation of styrene on TiO_2 and TiO_2/reduced graphene oxide (TiO_2/rGO) surface is compared under dry air condition to investigate the role of $\cdot O_2^-$ in styrene degradation. TiO_2/rGO shows 4.8 times higher degradation efficiency than that of TiO_2, resulting in 16% reduced production of intermediates with identical composition. The improved formation of $\cdot O_2^-$ on TiO_2/rGO is confirmed responsible for these variations. Theoretical calculation further reveals the enhancement of $\cdot O_2^-$ thermodynamically favoring conversion of styrene to acetophenone, turning the most dominant intermediate from benzoic acid on TiO_2 to acetophenone on TiO_2/rGO. The accumulated formation of acetophenone on TiO_2/rGO poses increased acute threat to human beings. Our findings proclaim that ROS promoted photocatalytic performance of semiconductor after carbon material composition ultimately changes the priority order of degradation pathways to form by-product with higher threat toward human beings. And more attentions are advised focusing on the relevance with degradation efficiency, intermediate and toxicity of aromatic hydrocarbons on carbon material based photocatalyst.

1. Introduction

Atmospheric pollution is still serious in urban cities of China at present (Huang et al., 2014; Jerrett, 2015), although great success has been achieved during last decade via the toughest-ever Air Pollution Prevention and Control Action Plan promulgated by State Council of China (Zhang et al., 2019a). The anthropogenic emission volatile organic compounds (VOCs) contribute importantly to atmospheric pollution and human health threat in cities (Wang et al., 2007). Aromatic hydrocarbons (AHs) account for 20%–30% of artificial VOCs (Ji et al., 2017). Therefore, how to effectively reduce the emission of AHs from anthropogenic source is a big challenge in China to cut down the threat of them to human living environment and resident health from now and in the time to come.

TiO_2 photocatalysis technology has been proved possessing elimination ability toward AHs from anthropogenic source (Chen et al., 2013, 2016, 2017; Lin et al., 2007; Wang et al., 2013; Zhang et al., 2019b). However, low degradation efficiency is always observed for pure TiO_2 (An et al., 2012; Khalil et al., 2019; Mei et al., 2020; Weon and Choi, 2016; Weon et al., 2018), due to producing limited reactive oxygen species (ROS). TiO_2 coupled by carbon material shows enhanced ROS and then improved photocatalytic performance of AHs (Andryushina and Stroyuk, 2014; Roso et al., 2015; Zhang et al., 2010). The contribution of each ROS (e.g., $\cdot OH$, $\cdot O_2^-$) to the improved performance are still confused. For instance, $\cdot OH$ and $\cdot O_2^-$ are reported playing equal contributions to the enhanced photocatalytic degradation efficiency of

* Corresponding author. Guangzhou Key Laboratory of Environmental Catalysis and Pollution Control, Key Laboratory of City Cluster Environmental Safety and Green Development, School of Environmental Science and Engineering, Guangdong University of Technology, Guangzhou, 510006, China.
E-mail address: antc99@gdut.edu.cn (T. An).

https://doi.org/10.1016/j.envres.2021.110747
Received 12 December 2020; Received in revised form 25 December 2020; Accepted 11 January 2021
Available online 19 January 2021
0013-9351/

o-xylene on TiO_2/reduced graphene oxide (TiO_2/rGO) (Lin et al., 2018), while $\cdot O_2^-$ exhibits more important role in the increased degradation activity to p-xylene than ·OH on the same catalyst (Zhang et al., 2019b). These confused conclusions also result in unclear contribution of ROS to the alternation of degradation pathways. Lin et al. deduced higher contribution of ·OH than $\cdot O_2^-$ to altered degradation steps of o-xylene on TiO_2/rGO (Lin et al., 2018). Recently, our work confirmed more important role of $\cdot O_2^-$ than ·OH in the transformation of n-hexane to epoxidation products on TiO_2 based catalyst (Wei et al., 2019). The altered degradation pathway may lead to formation of intermediate with high health risk. Unfortunately, same as degradation performance, the contribution of these ROS to the varied degradation mechanism as well as risk evolution of AHs is also unknown. Therefore, clarification of relationship between degradation performance and mechanism of AHs induced by different ROS becomes necessary for comprehensively understanding their photocatalytic degradation fate and health impact.

In this work, photocatalytic degradation of styrene on TiO_2 and TiO_2/rGO were comparably investigated under dry air condition. Styrene is selected as model AH, since it is a commercially important chemical widely used in the manufacture of synthetic rubber, resins, polyesters and plastics (An et al., 2012). Thus, unilateral regulation of $\cdot O_2^-$ on TiO_2 and TiO_2/rGO was achieved to study the contribution of these ROS to degradation performance and mechanism of styrene under dry air condition with limited ·OH and abundant $\cdot O_2^-$. Firstly, the degradation and mineralization performances of TiO_2 and TiO_2/rGO were evaluated, while the degradation intermediates of styrene on TiO_2 and TiO_2/rGO were compared via a gas chromatography-mass spectrometer (GC-MS). Two main ROS, including ·OH and $\cdot O_2^-$, generated from the surfaces of TiO_2 and TiO_2/rGO were characterized. And the effect of ROS on the degradation performance and intermediate properties (including composition, concentration and risk) was assessed. Finally, the relationship of ROS variation, degradation performance with intermediates' property was well established.

2. Experimental

2.1. Photocatalyst synthesis

The materials and reagents used in this study were directly used without pretreatment (Table S1). Graphene oxide (GO) was obtained from modified Hummer's method as reported in previous works (Chen et al., 2015; Li et al., 2013). The GO and commercial tetrabutyl titanate was separately dissolved in 30 mL of anhydrous ethanol and distilled water (volume ratio of 1:1) solution, and then was ultrasonicated for 1 h. The obtained GO solution was dropwise added into tetrabutyl titanate one and stirred for 30 min before transferred into 100 mL of Teflon-lined stainless steel autoclave. The autoclave was then heated to 160 °C and maintained for 24 h. After cooling off, the sediment was centrifuged, rinsed with distilled water and freeze dried, and the obtained composite was denoted as TiO_2/rGO. For the comparison, TiO_2 was also fabricated with the same method without the addition of GO.

Raman spectrum of TiO_2/rGO was recorded on a LabRAM HR Evolution high spectral resolution confocal Raman microscope with a laser excitation wavelength of 532 nm, which confirmed the co-existence of TiO_2 (148, 397, 520 and 636 cm^{-1}) and rGO (1343 and 1602 cm^{-1}) in the composite (Figure S1a). The weight content of rGO in TiO_2/rGO was determined by a Thermogravimetric analyzer (STA 409 PC), which revealed rGO weight percentage of ca. 4% (Figure S1b). UV–visible (UV–Vis) absorption spectra of TiO_2 and TiO_2/rGO were recorded on a UV-vis-NIR spectrophotometer (Varian Cary 300). The presence and mobility of oxygen species on TiO_2 and TiO_2/rGO were studied by using temperature-programmed desorption of oxygen (O_2-TPD) performed on a TP-5078 multifunction adsorption instrument. The fluorescence spectra of TiO_2 and TiO_2/rGO were collected by using a Fluorolog-3 fluorescence spectrophotometer with an excitation wavelength of 321 nm at wavelengths between 330 and 600 nm, while the photoluminescence decay lifetimes of them were calculated based on previous method (Jin et al., 2013; Xu et al., 2017).

2.2. Photocatalytic degradation experiment

The photocatalytic performances of TiO_2 and TiO_2/rGO were evaluated using gaseous styrene as a model pollutant in a continuous flow reactor as reported in our previous works (Chen et al., 2013, 2014; Liu et al., 2019). In a typical process, 20 ppmv of styrene was fed into the reactor loading 100 mg of TiO_2 or TiO_2/rGO with a flow rate of 60 mL min^{-1} by dry air. The relative humidity (RH) of reaction gas was measured at 5%. A 300 W xenon lamp (PLS-SXE300C) was used as a light source fixed vertically on top of the reactor with a distance of 20 cm. The light intensity was measured as 100 mW cm^{-2}. Before the lamp was switched on, the adsorption equilibrium was acheived. The concentrations of styrene and CO_2 at the outlet were analyzed by a gas chromatograph (GC-9800) equipped with flame ionization detector and methane converter. The column temperature, injector temperature and detector temperature of GC were set as 150 °C, 130 °C and 200 °C, respectively. Direct photolysis does not lead to decrease of styrene concentration. At 240 and 480 min, the catalyst was taken out for further intermediate analysis on its surface.

2.3. Intermediate identification and quantification analysis

The formed intermediates on TiO_2 and TiO_2/rGO were extracted with methanol via our reported method (An et al., 2011). The filtrate was collected, concentrated, dried with high-purity nitrogen and diluted to 1 mL with ethyl acetate. The diluted sample was injected into GC-MS (Agilent 7890B–5977B) for analysis. A DB-4MS capillary column (60 m × 0.32 mm × 0.25 μm) was used with GC oven temperature program: initially 40 °C for 5 min, programmed to 160 °C at a rate of 5 °C min^{-1}, then to 280 °C at a rate of 10 °C min^{-1} and held for 2 min. Mass spectrometer conditions were set as follows: temperature of transfer line of 280 °C, ionizing energy of 70 eV and scan range of 45–260 me^{-1}.

The concentration of intermediate was obtained based on calibration curve method (Chen et al., 2020). As shown in Figure S2, the designed concentrations of benzaldehyde (20, 40, 80, 160 and 240 ppm), benzyl alcohol (15, 20, 30, 40 and 50 ppm), acetophenone (5, 10, 20, 50 and 100 ppm), methyl mandelate (20, 30, 50, 80 and 100 ppm) and benzoic acid (50, 80, 100, 150 and 200 ppm) were obtained after dissolving in ethyl acetate. Then, 1 mL of the above standard sample was transferred to clean cell bottle for GC-MS analysis. The GC-MS analysis conditions for these standard samples were identical as the detection of intermediates.

2.4. ROS characterization on TiO_2 and TiO_2/rGO

For qualitative analysis of ·OH and $\cdot O_2^-$ generated on TiO_2 and TiO_2/rGO, an electron paramagnetic resonance spectrometer (EPR, EMXplus-10/12) method was employed. Typically, 100 mg of catalyst was added into 100 mM of 5,5-dimethyl-1-pyrroline N-oxide (DMPO) acetonitrile solution. Then, a certain amount of water was added to simulate 5% RH. After 10 min's irradiation, 1 mL of solution was taken out, filtered, capillary sampled and measured.

2.5. Theoretical calculation of ROS involved degradation mechanism of styrene

The quantum chemical calculation of reaction energy for ROS involved degradation mechanism of styrene was conducted by Gaussian 09 package (Li et al., 2019; Wei et al., 2019). The reactants and intermediates were geometrically optimized by using density functional theory (Ji et al., 2017). The hybrid density functional M06-2X/6-311G (d, p) level was adopted. The dual-level potential profile was refined at M06-2X/6–311 t G (3df, 3pd) level. The dual level approach was

assigned as X//Y, where a single-point energy calculation at level X was carried out for the geometry optimized at a lower level Y (M06-2X//M06-2X).

2.6. Acute risk evaluation of intermediates obtained via different pathways

The acute risk of intermediates was evaluated to investigate their potential acute effects on human beings after short-time contact. The intermediate risk quotient (RQ) was the ratio of its mass (mg) and 50% lethal dose (LD_{50} × 70 kg of human body). Then, the RQs of intermediates generated through different pathways on both TiO_2 and TiO_2/rGO were calculated and compared.

3. Results and discussion

3.1. Degradation and mineralization efficiency of styrene on TiO_2 and TiO_2/rGO

The adsorption of pollutants onto the photocatalyst surface is the first step of photocatalytic reaction, which may influence later degradation and mineralization efficiency (Zhang et al., 2006). And graphene shows excellent adsorption ability toward AHs (Kim et al., 2018; Yu et al., 2018; Zhang et al., 2017). In this work, the adsorption behaviors of styrene on TiO_2 and TiO_2/rGO are first compared to reveal the contribution of rGO to the adsorption performance of TiO_2. As seen from Fig. 1a, the outlet concentration of styrene after adsorbed by TiO_2 sharply decreases from 20 to 5.8 ppmv within 10 min, and achieves adsorption-desorption equilibrium within 470 min and then back to initial concentration. The fast adsorption and slow equilibrium curve with V-shape indicates the enrichment of styrene on TiO_2, facilitating later surface degradation. The V-shape curve is also observed for styrene adsorption on TiO_2/rGO with the lowest outlet concentration of 3.9 ppmv within 20 min with the equilibrium time of 880 min. The lower outlet concentration and longer equilibrium time of TiO_2/rGO than TiO_2 indicate higher adsorption ability. The enhanced adsorption capacity of TiO_2 by graphene toward other AHs is also observed in previous works (Lin et al., 2018; Yue et al., 2019), confirming our results.

After achievement of adsorption and desorption equilibrium, Xe lamp is switched on and the degradation is began. As shown in Fig. 1b, the concentration of styrene at the outlet sharply increases from 20 to 41.6 ppmv on TiO_2 and to 277.3 ppmv on TiO_2/rGO within 5 min. This is because that the catalyst absorbs the infrared light of Xe lamp to heat itself up, resulting in instant desorption of enriched styrene from catalyst surface. Our previous works also observed the similar phenomenon (Liu et al., 2019; Yao et al., 2018). The much higher concentration of desorbed styrene from TiO_2/rGO than TiO_2 again confirms the enhanced adsorption performance by rGO. After instant desorption process, the outlet concentration of styrene starts to decrease, suggesting that the photocatalysis begins to work. In the case of TiO_2, around 6.8 ppmv of styrene is detected at the outlet within 30 min, corresponding to degradation efficiency of 66%. And outlet styrene concentration gradually increases to 19.1 ppmv within 600 min with the degradation efficiency accordingly reducing to 5%. This much low degradation efficiency implies almost deactivation of TiO_2 within 600 min, revealing that TiO_2 shows unstable solar-light-driven photocatalytic degradation performance toward styrene in this study. Our previous works also reported the deactivation phenomenon of TiO_2 toward styrene degradation (An et al., 2012; Chen et al., 2014), agreeing with current result. Similar deactivation phenomenon of TiO_2 toward other AHs, such as benzene (Uner and Ozbek, 1999), toluene (Weon et al., 2018), are also observed, further supporting our conclusion than TiO_2 catalyst alone can easily be deactivated when treating AHs. The combining of graphene composition with TiO_2 is an efficient method to promote degradation activity and stability of TiO_2. As seen from Fig. 1b, the outlet concentration of styrene initially decreases to 5.9 ppmv (with 71% of degradation efficiency) within 100 min and then gradually increases to 11.3 ppmv (with 44% of degradation efficiency) within 600 min on TiO_2/rGO. Both degradation activity and stability are improved for TiO_2/rGO catalyst in comparison with TiO_2. Ebrahimi and Fatemi also reported the promoted photocatalytic degradation of gaseous acetaldehyde on TiO_2/rGO than TiO_2 (Ebrahimi and Fatemi, 2017), consistent with our result. Besides degradation performance, the enhanced mineralization activity and stability of TiO_2 by rGO is also obtained. Within 600 min, the mineralization of styrene on TiO_2 and TiO_2/rGO generates 7.3 and 30.1 ppmv of CO_2, corresponding to 4% and 19% of mineralization efficiencies of styrene (Fig. 1c).

3.2. Altered production of intermediate by enhanced degradation performance

Different degradation and mineralization efficiencies of styrene on TiO_2 and TiO_2/rGO may result in the production of different intermediates. To verify this assumption, TiO_2 and TiO_2/rGO after reaction for 240 min are taken out from the reactor, extracted and the extraction solution is injected into GC-MS for intermediate analysis. As for TiO_2 and TiO_2/rGO, a total of four peaks (No. 1–4) are observed with the retention time of 4.84, 7.22, 7.95 and 16.70 min respectively (Figure S2a), indicating the formation of same intermediates on these two catalysts. After comparing the mass fragment information listed in Table 1 with NIST database and standard samples (Figure S3), these four intermediates are identified as benzaldehyde, benzyl alcohol, acetophenone and methyl mandelate. The degradation of styrene to benzaldehyde, benzyl alcohol and acetophenone is also observed on TiO_2 under UV irradiation in a fixed bed reactor (Chen et al., 2019), partially proving current result. Methyl mandelate is one of esters, and its formation suggests the happening of esterification reaction of styrene on TiO_2 and TiO_2/rGO under solar light irradiation. Notably, this is the first time to report the photochemical esterification transformation of styrene to the ester intermediate on TiO_2.

Further prolonging degradation time to 480 min leads to new formation of benzoic acid (No. 5 intermediate, with the retention time of 13.06 min) on TiO_2 and TiO_2/rGO (Table 1 and Figure S2b), indicating further transformation of formed intermediate (e.g., benzaldehyde) to this compound. The photocatalytic degradation of benzaldehyde to benzoic acid has also been reported for other AHs on TiO_2 (Blount and

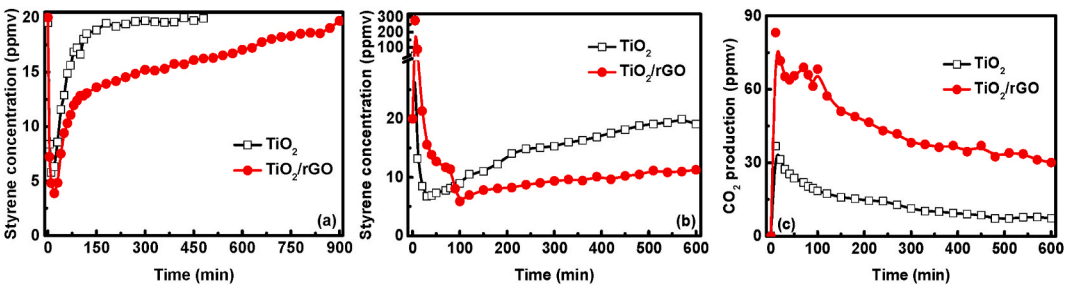

Fig. 1. Adsorption (a), photocatalytic degradation (b) and CO_2 production (c) kinetics curves of styrene on TiO_2 and TiO_2/rGO.

Table 1
Name, formula, retention time, structure and main fragment of intermediates adsorbed on TiO_2 and TiO_2/rGO.

NO.	Name	Formula	**Retention time (min)**	Structure	Main fragments (m/z)
1	Benzaldehyde	C_7H_6O	4.84	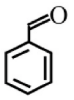	106, 77, 51
2	Benzyl alcohol	C_7H_8O	7.22		108, 91, 79, 51
3	Acetophenone	C_8H_8O	7.95		120, 105, 77, 51
4	Methyl mandelate	$C_9H_{10}O_3$	16.70	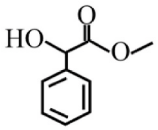	166, 107, 79, 51
5	Benzoic acid	$C_7H_6O_2$	13.06	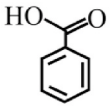	122, 105, 77, 51

Falconer, 2001; Guo et al., 2008; Mendez-Roman and Cardona-Martinez, 1998), agreeing with our hyphothesis. The detection of bezoinc acid at 480 min rather than at 240 min suggests that the transformation of benzaldehyde to benzoic acid may begin after 240 min or the concentration of formed benzoic acid at 240 min is too low to be deteced by GC-MS. Anyway, the same intermediate formation on TiO_2 and TiO_2/rGO at 240 and 480 min indicates negligible impact of enhanced degradation performance by rGO coupling to the composition of by-products formed on TiO_2. However, further compare reveal different peak intensities of same intermediates on TiO_2 and TiO_2/rGO, suggesting different concentrations of them on these two catalysts. The quantification of intermediates are conducted through the calibration curve method. Figure S4 shows the calibration curves of five standard samples. The calibration curve correlation coefficients (R^2) for all selected samples exceed 0.9975 within the investigated concentration ranges, suggesting the reliability of the calibration curves. And after calculating the peak areas of intermediates with the equations from calibration curves, the mass of each intermediate is obtained and listed in Tables S2 and S3, and the total mass of intermediates is also displayed in Fig. 2a.

About 59.60 and 76.30 mg of intermediates in total are generated on TiO_2 and TiO_2/rGO from degradation of styrene at 240 min. Higher concentrated intermediates on TiO_2/rGO is resulted from degradation of more adsorbed styrene (see Fig. 1a). Among these intermediates, methyl mandelate contributes the highest percentage of mass for both TiO_2 (53.00%) and TiO_2/rGO (44.73%) (Fig. 2b), suggesting the dominant transformation of styrene to this ester within 240 min. The followed are benzaldehyde (21.94%), benzyl alcohol (14.05%) and acetophenone (11.01%) for TiO_2. Differently, acetophenone contributes higher percentage of mass (28.81%) than benzaldehyde (13.30%) and benzyl alcohol (13.17%) on TiO_2/rGO. Our published result also confirmed different degradation pathways of styrene to benzaldehyde and acetophenone on TiO_2 (Chen et al., 2019). The altered percentage ranking of mass from benzaldehyde to acetophenone indicates that rGO enhanced degradation performance ultimately changes the formation priority of intermediates.

Prolonging reaction time leads to further alteration of intermediate mass and percentage ranking. As shown in Fig. 2a, continuous degradation of styrene within 480 min results in the formation of 277.49 and 238.98 mg of products on TiO_2 and TiO_2/rGO. And 4.65 and 3.13 times higher mass of intermedates were obtained at 480 min than that at 240 min suggests the significant accumulation of intermediates along with the reaction time. Further comparison shows that higher percentage of intermediate is formed on TiO_2/rGO (78.52%) than on TiO_2 (68.07%) within the second 240 min, consistent with faster decreased degradation efficiency of the latter than the former (Fig. 1b). Moreover, less intermediates are formed on TiO_2/rGO than on TiO_2 at 480 min in comparison with that at 240 min, suggesting that the enhanced degradation performance by rGO prohibits the intermediate formation within enough degradation time. The improved generation of CO_2 on TiO_2/rGO than on TiO_2 solidly confirms this prohibition (Fig. 1c).

Among the obtained five intermediates on TiO_2 at 480 min, benzoic acid contributes the highest percentage (40.32%), and followed are methyl mandelate (23.15%), acetophenone (18.97%), benzyl alcohol (8.90%) and benzaldehyde (8.66%). This result indicates dominant formation of benzoic acid on TiO_2 from styrene degradation at 480 min.

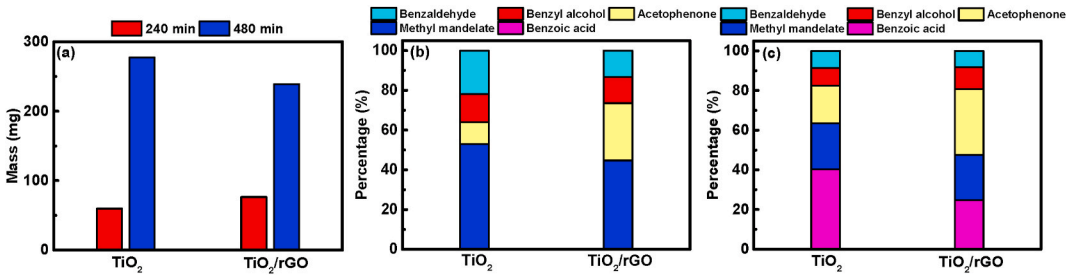

Fig. 2. Mass of total intermediates (a), and their percentages on TiO_2 and TiO_2/rGO at 240 (b) and 480 min (c).

Lower percentage of mass for benzoic acid is obtained on TiO_2/rGO (24.70%), reveals that rGO efficiently suppresses the formation of benzoic acid on TiO_2. Unexpectedly, acetophenone shows the highest percentage of mass (33.22%) than benzoic acid, methyl mandelate (22.72%), benzyl alcohol (11.05%) and benzaldehyde (8.31%) on TiO_2/rGO. These results again confirm the altered intermediate percentage ranking on TiO_2 by rGO coupling.

3.3. Effect of ROS enhanced degradation performance to oxidation mechanism of styrene

As known, photogenerated h^+ and e^- can activate H_2O and O_2 molecules to form ROS such as ·OH and $\cdot O_2^-$ (see Eqs. 1-4), which then play important roles in photocatalysis.

$$\text{Catalyst} + h\nu \rightarrow h^+ + e^- \quad (1)$$

$$H_2O + h^+ \rightarrow \cdot OH + H^+ \quad (2)$$

$$O_2 + e^- \rightarrow \cdot O_2^- \quad (3)$$

EPR results shown in Fig. 3a reveal different variation of these ROS on the surface of TiO_2 and TiO_2/rGO catalysts. No ·OH–DMPO signal is detected in both TiO_2 and TiO_2/rGO photocatalytic systems (Figure S5). This may be because that low H_2O content in this study (5% RH) results in too low concentrated ·OH to be detected by EPR. Conversely, clear $\cdot O_2^-$–DMPO signals are observed in both systems. Meanwhile, TiO_2/rGO displays 1.9 times stronger intensity of $\cdot O_2^-$ signal than TiO_2. Further O_2-TPD results reveal the enhanced O_2 desorption on TiO_2/rGO than TiO_2 (Fig. 3b), indicating more enrichment of O_2 with coupling with rGO composition. In addition, the fluorescence spectra shows that the PL intensity of TiO_2/rGO is much lower than that of TiO_2 (Fig. 3c), indicating that the former possesses higher separation efficiency of photogenerated h^+ and e^-. Moreover, shorter PL lifetime of TiO_2/rGO (2.51 ns) than TiO_2 (3.03 ns) is obtained from time-resolved PL spectrum (Fig. 3d), indicating faster charge transfer and separation efficiency of TiO_2 after rGO coupling. Then, the increased e^- concentration on TiO_2/rGO reduces higher concentrated O_2 to form more $\cdot O_2^-$. In all, in comparison with ·OH, the enhanced $\cdot O_2^-$ contributes to higher degradation and mineralization performances of TiO_2/rGO than TiO_2. To further understand the effect of $\cdot O_2^-$ enhanced photocatalytic performance to the oxidation mechanism, ROS involved quantum chemical calculations are also employed with intermediate data (Fig. 4). Beside $\cdot O_2^-$, ·OH is also involved in the calculation, although it shows very low concentration.

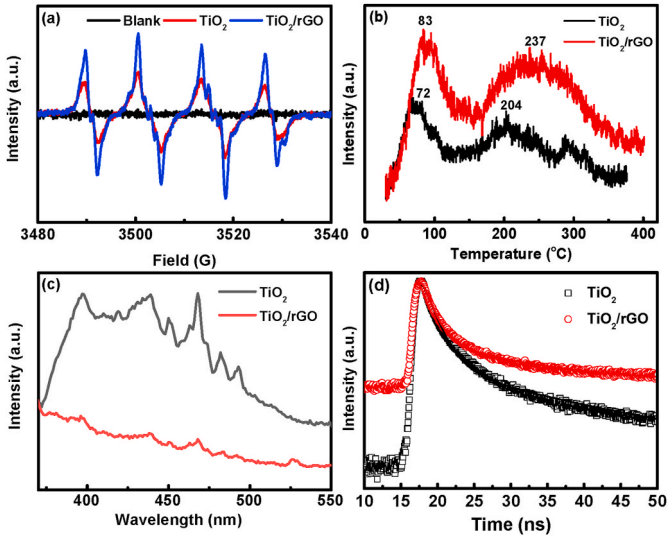

Fig. 3. EPR spectrum (a), O_2-TPD profile (b), steady-state (c) and time-resolved (b) PL spectra of TiO_2 and TiO_2/rGO.

Firstly, the reaction of styrene with ·OH only is investigated. Addition of one ·OH onto C═C bond of styrene leads to formation of 1-phenylethyl alcohol radical, with releasing energy of 27.71 kcal mol^{-1}. This radical further reacts with three ·OH to form 2-hydroxy-2-phenylacetaldehyde after losing two H_2O. About 206.26 kcal mol^{-1} of energy is released from this reaction, indicating a thermodynamically favorable process. Under further attack by two ·OH at carbonyl group of the aldehyde, the accordingly aromatic acid, 2-hydroxy-phenylacetic acid, is obtained after losing one H_2O. Our theoretically calculated reaction energy of −138.22 kcal mol^{-1} reveals the spontaneous transformation from 2-hydroxy-2-phenylacetaldehyde to 2-hydroxy-phenylacetic acid with the presence of sufficient ·OH. Then, the acid reacts with one methanol to form methyl mandelate. This esterification process releases about 5.49 kcal mol^{-1} of energy, indicating spontaneous formation of methyl mandelate. The transformation process of styrene to methyl mandelate is named as pathway I.

In addition to direct attack by ·OH, 1-phenylethyl alcohol radical also undergoes a rearrangement reaction. The theoretical calculation of reaction energy reveals that this is a spontaneous process ($\triangle E_r = -19.53$ kcal mol^{-1}). Under further attack by ·OH, the rearranged radical is converted into acetophenone, releasing significantly high energy ($\triangle E_r = -83.56$ kcal mol^{-1}). This process is named as pathway II. The much higher energy released from pathway I (377.68 kcal mol^{-1}) than pathway II (130.80 kcal mol^{-1}) reveals the preferential transformation of styrene to methyl mandelate under the condition of enough ·OH.

The C═C bond of styrene can be broken by ·OH to form ethylbenzene. The release of 46.38 kcal mol^{-1} of energy confirms the spontaneous happening of this breaking process. Our recent work also observed the formation of ethylbenzene from the degradation of styrene with the presence of ·OH (Chen et al., 2019), consistent with current result. Furthermore, ·OH abstracts H atom of methyl group of ethylbenzene to generate benzyl alcohol after losing one methyl radical, accompanying with the released energy of 5.30 kcal mol^{-1}. The benzyl alcohol then transforms to benzaldehyde and benzoic acid after two steps of H abstraction reactions by ·OH, releasing energies of 117.54 and 67.70 kcal mol^{-1} respectively. These high released energies reveal easily happening of above two processes. The conversion process of styrene to benzoic acid is then named as pathway III. The possible degradation of ethylbenzene successively to benzyl alcohol, benzaldehyde and benzoic acid by ·OH is also deduced by Cheng et al. (2013), well aggreeing with our results.

Clearly, styrene separately undergoes three pathways to finally form methyl mandelate, acetophenone or benzoic acid. Reaction energy results indicate that when only reaction with ·OH, pathway I releases energy of 377.68 kcal mol^{-1}, which is 2.89 and 1.59 times higher than pathway II (130.80 kcal mol^{-1}) and pathway III (236.92 kcal mol^{-1}). Meanwhile, methyl mandelate, final product of pathway I, accounts for the highest percentage on TiO_2 (53.00%) and TiO_2/rGO (44.73%) at 240 min. These results suggest that styrene thermodynamically favors the transformation to methyl mandelate through pathway I under the effect of sufficient ·OH within initial 240 min's reaction. However, longer reaction time with ·OH decreases the mass percentage of methyl mandelate on both TiO_2/rGO and TiO_2, implying that degradation styrene via pathway I should be influenced by other radicals, such as $\cdot O_2^-$. The EPR result confirms the promoted intensity of $\cdot O_2^-$ on TiO_2/rGO than TiO_2, while the lifetime of $\cdot O_2^-$ (*ca.* 5 s) is 25 times longer than that of ·OH (*ca.* 0.2 s) (Wang et al., 2017). Then, longer reaction time prefers the accumulation of higher concentrated $\cdot O_2^-$ than ·OH on TiO_2 and TiO_2/rGO surfaces.

In order to reveal the effect of $\cdot O_2^-$ to the degradation pathway, ·OH is gradually replaced by $\cdot O_2^-$ for reaction energy calculation. Since ·OH inevitably participates in the degradation process due to its high reactivity, the processes containing two or more ·OH is selected for the replacement reactions. Based on this criterion, ·OH in followed processes is replaced by $\cdot O_2^-$: from 1-phenylethyl alcohol radical to 2-hydroxy-2-phenylacetaldehyde and 2-hydroxy-2-phenylacetaldehyde to

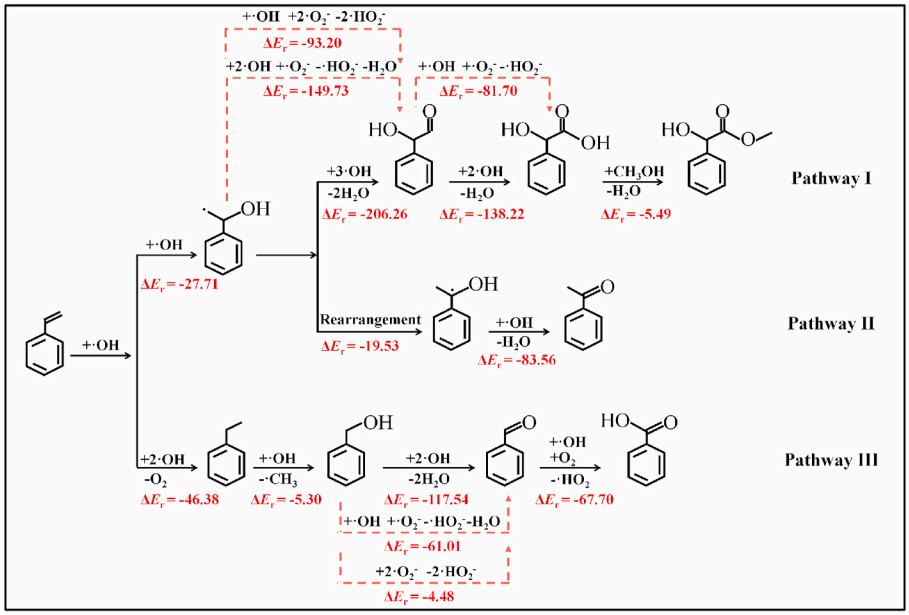

Fig. 4. ·OH and $\cdot O_2^-$ involved photocatalytic degradation pathway of styrene.

2-hydroxy-phenylacetic acid in pathway I, and benzyl alcohol to benzaldehyde in pathway III.

As shown in Fig. 4, when one ·OH is replaced by one $\cdot O_2^-$, the released energies of above three processes are theoretically calculated as the energy of 149.73, 81.70 and 61.01 kcal mol^{-1}, resulting in the total released energies of 264.63 kcal mol^{-1} for pathway I and 180.39 kcal mol^{-1} for pathway III. The decreased energy disparity between these two pathways from 140.76 to 84.24 kcal mol^{-1} implies that the $\cdot O_2^-$ prefers to suppress the happening of pathway I rather than pathway III, leading to the enhanced formation of benzoic acid product. The increased percentage of benzoic acid from 0 to 40.32% on TiO_2 and to 24.70% on TiO_2/rGO at 480 min solidly confirms this hypothesis. Further comparison shows higher percentage of intermediates on TiO_2/rGO than TiO_2 via pathway II (33.22% > 18.97%) at 480 min, while lower ones via pathway I (22.72% < 23.15%) and pathway III (44.06% < 57.88%) are obtained. These results suggest preferential occurrence of pathway II than other two pathways on TiO_2/rGO when more $\cdot O_2^-$ participating in the degradation process. Theoretical calculations of two ·OH replaced by two $\cdot O_2^-$ reveal further decreased energies of pathway I to 208.10 kcal mol^{-1} and pathway III to 123.86 kcal mol^{-1}, proving above results. Therefore, styrene prefers the transformation to methyl mandelate on both TiO_2 and TiO_2/rGO via pathway I in the presence of ·OH, while it is favorably converted to benzoic acid on TiO_2 or to acetophenone on TiO_2/rGO through pathway III or II in the presence of sufficient $\cdot O_2^-$.

3.4. Acute risk evolution for styrene oxidation pathways on TiO_2 and TiO_2/rGO

Since alternation of $\cdot O_2^-$ leads to different variation of concentration and percentage of various intermediates, they may result in different health risk to human beings after diffused into the atmosphere. Here, the total acute risks of intermediates generated via three pathways are calculated and compared (Fig. 5). The results found that total RQs of 4.35×10^{-4} and 6.80×10^{-4} are obtained from intermediates on TiO_2 and TiO_2/rGO at 240 min (Fig. 5a). The higher RQ on TiO_2/rGO than on TiO_2 indicates that enhanced health threat of intermediates on TiO_2 after rGO composition within initial reaction period. The increased production of intermediates contributes to the enhanced health risk (Fig. 2a). The 3.3 times higher RQ of acetophenone generated via pathway II on TiO_2/rGO than on TiO_2 is responsible for enhancement of total health risk, since RQs of intermediates produced through pathway I and pathway III on TiO_2 (1.33×10^{-4} and 2.05×10^{-4}) and TiO_2/rGO (1.43×10^{-4} and 2.09×10^{-4}) almost equal. These results reveal that rGO accelerates formation of intermediate with higher health risk on TiO_2.

Degradation of styrene on TiO_2 and TiO_2/rGO for another 240 min leads to further increased RQ to 2.29×10^{-3} and 2.30×10^{-3}, indicating the enhanced health risk of by-products to human beings with extended reaction time. The accumulation of intermediates contributes to this enhancement (Fig. 2a). Notably, lower mass of intermediates on TiO_2/rGO displays equal RQ to TiO_2, again suggesting production of intermediate with high health risk on the former. Detail analysis reveals close

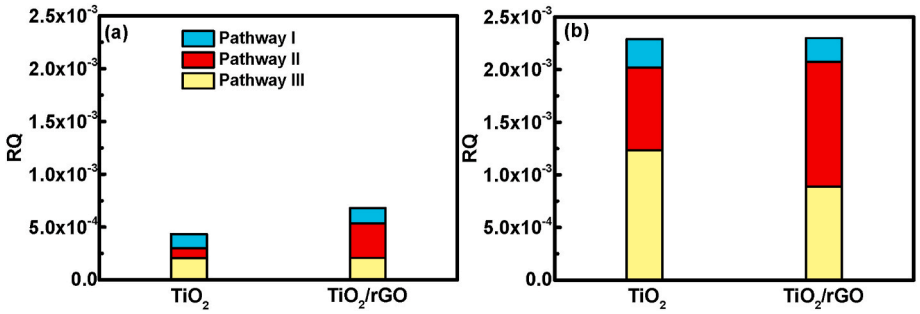

Fig. 5. RQ of total intermediates from pathway I, II and III on TiO_2 and TiO_2/rGO at 240 (a) and 480 min (b).

RQs on TiO_2 (2.70×10^{-4}) and TiO_2/rGO (2.28×10^{-4}) for intermediates obtained via pathway I, while lower RQ is observed on TiO_2/rGO (8.90×10^{-4}) than TiO_2 (1.24×10^{-3}) for intermediates from pathway III (Fig. 5b). These results indicate that intermediates from these two pathways do not contribute to above high risk. However, it is found that the highest RQ of intermediates on TiO_2 and TiO_2/rGO belongs to pathway III and pathway II, indicating that rGO coupling alters the contribution of degradation pathway to RQ on TiO_2. Acetophenone generated through pathway II displays 1.5 times higher RQ on TiO_2/rGO than TiO_2. Hence, rGO composition facilitates the formation of acetophenone with high acute risk through pathway II. Obviously, the presence of rGO efficiently changes the acute risk contribution of intermediates that more attentions should be refocused on evaluation of toxicity of intermediates on carbon material based photocatalyst as well as mechanism of toxicity variation.

4. Conclusion

In this study, enhanced degradation and mineralization performances of styrene on TiO_2/rGO than TiO_2 were obtained, mainly due to the promoted $\cdot O_2^-$ formation after rGO composition coupling with TiO_2. The rGO addition did not alter the kind of degradation intermediates, but reduced the mass of formed intermediates on TiO_2. Styrene was preferentially converted to benzoic acid on TiO_2 and to acetophenone on TiO_2/rGO in the presence of sufficient $\cdot O_2^-$. The dominant RQ contribution was altered from benzoic acid to acetophenone, revealing that rGO composition addition facilitated the formation of acetophenone, which then showed the increased acute threat to human beings. Our findings suggested the increased photocatalytic performance and decreased intermediate formation after carbon material composition to semiconductor, which might also lead to the formation of by-product with higher risk to human beings.

Author statement

Jiangyao Chen: Formal analysis, Methodology, Writing – original draft. Zilong Zhang: Formal analysis, Methodology. Weikun Zhu: Investigation. Liyun Zhang: Investigation. Baocong Zhao: Investigation. Yuemeng Ji:Data curation. Guiying Li:Validation. Taicheng An: Conceptualization, Supervision.

Declaration of competing interest

The authors declare that they have no known competing financial interests or personal relationships that could have appeared to influence the work reported in this paper.

Acknowledgement

This work was financially supported by Key-Area Research and Development Program of Guangdong Province (2019B110206002), National Key R&D Program of China (2019YFC0214402 and 2019YFC1804503), National Natural Science Foundation of China (21777032), Local Innovative and Research Teams Project of Guangdong Pearl River Talents Program (2017BT01Z032), and The Innovation Team Project of Guangdong Provincial Department of Education, China (2017KCXTD012).

Appendix A. Supplementary data

Supplementary data to this article can be found online at https://doi.org/10.1016/j.envres.2021.110747.

References

An, T.C., Chen, J.Y., Nie, X., Li, G.Y., Zhang, H.M., Liu, X.L., Zhao, H.J., 2012. Synthesis of carbon nanotube-anatase TiO_2 sub-micrometer-sized sphere composite photocatalyst for synergistic degradation of gaseous styrene. ACS Appl. Mater. Interfaces 4, 5988–5996.

An, T.C., Sun, L., Li, G.Y., Gao, Y.P., Ying, G.G., 2011. Photocatalytic degradation and detoxification of o-chloroaniline in the gas phase: mechanistic consideration and mutagenicity assessment of its decomposed gaseous intermediate mixture. Appl. Catal. B Environ. 102, 140–146.

Andryushina, N.S., Stroyuk, O.L., 2014. Influence of colloidal graphene oxide on photocatalytic activity of nanocrystalline TiO_2 in gas-phase ethanol and benzene oxidation. Appl. Catal. B Environ. 148, 543–549.

Blount, M.C., Falconer, J.L., 2001. Characterization of adsorbed species on TiO_2 after photocatalytic oxidation of toluene. J. Catal. 200, 21–33.

Chen, J.Y., He, Z.G., Ji, Y.M., Li, G.Y., An, T.C., Choi, W.Y., 2019. (OH)-O-center dot radicals determined photocatalytic degradation mechanisms of gaseous styrene in TiO_2 system under 254 nm versus 185 nm irradiation: combined experimental and theoretical studies. Appl. Catal. B Environ. 257, 117912.

Chen, J.Y., He, Z.G., Li, G.Y., An, T.C., Shi, H.X., Li, Y.Z., 2017. Visible-light-enhanced photothermocatalytic activity of ABO(3)-type perovskites for the decontamination of gaseous styrene. Appl. Catal. B Environ. 209, 146–154.

Chen, J.Y., Huang, Y., Li, G.Y., An, T.C., Hu, Y.K., Li, Y.L., 2016. VOCs elimination and health risk reduction in e-waste dismantling workshop using integrated techniques of electrostatic precipitation with advanced oxidation technologies. J. Hazard Mater. 302, 395–403.

Chen, J.Y., Li, G.Y., Zhang, H.M., Liu, P.R., Zhao, H.J., An, T.C., 2014. Anatase TiO_2 mesocrystals with exposed (001) surface for enhanced photocatalytic decomposition capability toward gaseous styrene. Catal. Today 224, 216–224.

Chen, J.Y., Nie, X., Shi, H.X., Li, G.Y., An, T.C., 2013. Synthesis of TiO_2 hollow sphere multimer photocatalyst by etching titanium plate and its application to the photocatalytic decomposition of gaseous styrene. Chem. Eng. J. 228, 834–842.

Chen, J.Y., Yi, J.J., Ji, Y.M., Zhao, B.C., Ji, Y.P., Li, G.Y., An, T.C., 2020. Enhanced H-abstraction contribution for oxidation of xylenes via mineral particles: implications for particulate matter formation and human health. Environ. Res. 186, 109568.

Chen, J.Y., Zhang, H.M., Liu, P.R., Li, Y.B., Liu, X.L., Li, G.Y., Wong, P.K., An, T.C., Zhao, H.J., 2015. Cross-linked $ZnIn_2S_4$/rGO composite photocatalyst for sunlight-driven photocatalytic degradation of 4-nitrophenol. Appl. Catal. B Environ. 168, 266–273.

Cheng, Z.W., Feng, L., Chen, J.M., Yu, J.M., Jiang, Y.F., 2013. Photocatalytic conversion of gaseous ethylbenzene on lanthanum-doped titanium dioxide nanotubes. J. Hazard Mater. 254, 354–363.

Ebrahimi, A., Fatemi, S., 2017. Titania-reduced graphene oxide nanocomposite as a promising visible light-active photocatalyst for continuous degradation of VVOC in air purification process. Clean Technol. Environ. Policy 19, 2089–2098.

Guo, T., Bai, Z.P., Wu, C., Zhu, T., 2008. Influence of relative humidity on the photocatalytic oxidation (PCO) of toluene by TiO_2 loaded on activated carbon fibers: PCO rate and intermediates accumulation. Appl. Catal. B Environ. 79, 171–178.

Huang, R.J., Zhang, Y.L., Bozzetti, C., Ho, K.F., Cao, J.J., Han, Y.M., Daellenbach, K.R., Slowik, J.G., Platt, S.M., Canonaco, F., Zotter, P., Wolf, R., Pieber, S.M., Bruns, E.A., Crippa, M., Ciarelli, G., Piazzalunga, A., Schwikowski, M., Abbaszade, G., Schnelle-Kreis, J., Zimmermann, R., An, Z.S., Szidat, S., Baltensperger, U., El Haddad, I., Prevot, A.S.H., 2014. High secondary aerosol contribution to particulate pollution during haze events in China. Nature 514, 218–222.

Jerrett, M., 2015. The death toll from air-pollution sources. Nature 525, 330–331.

Ji, Y.M., Zhao, J., Terazono, H., Misawa, K., Levitt, N.P., Li, Y.X., Lin, Y., Peng, J.F., Wang, Y., Duan, L., Pan, B.W., Zhang, F., Feng, X.D., An, T.C., Marrero-Ortiz, W., Secrest, J., Zhang, A.L., Shibuya, K., Molina, M.J., Zhang, R.Y., 2017. Reassessing the atmospheric oxidation mechanism of toluene. P. Natl. Acad. Sci. USA 114, 8169–8174.

Jin, S.Y., Son, H.J., Farha, O.K., Wiederrecht, G.P., Hupp, J.T., 2013. Energy transfer from quantum dots to Metal-Organic Frameworks for enhanced light harvesting. J. Am. Chem. Soc. 135, 955–958.

Khalil, A., Nasser, W.S., Osman, T.A., Toprak, M.S., Muhammed, M., Uheida, A., 2019. Surface modified of polyacrylonitrile nanofibers by TiO_2/MWCNT for photodegradation of organic dyes and pharmaceutical drugs under visible light irradiation. Environ. Res. 179, 108788.

Kim, J.M., Kim, J.H., Lee, C.Y., Jerng, D.W., Ahn, H.S., 2018. Toluene and acetaldehyde removal from air on to graphene-based adsorbents with microsized pores. J. Hazard Mater. 344, 458–465.

Li, J., Chen, J.Y., Ji, Y.M., Wang, J.X., Li, G.Y., An, T.C., 2019. Solar light induced transformation mechanism of allyl alcohol to monocarbonyl and dicarbonyl compounds on different TiO_2: a combined experimental and theoretical investigation. Chemosphere 232, 287–295.

Li, Y.B., Zhang, H.M., Liu, P.R., Wang, D., Li, Y., Zhao, H.J., 2013. Cross-linked g-C_3N_4/rGO nanocomposites with tunable band structure and enhanced visible light photocatalytic activity. Small 9, 3336–3344.

Lin, T., Pi, Z., Gong, M.C., Zhong, J.B., Wang, J.L., Chen, Y.Q., 2007. Gas-phase photocatalytic oxidation of benzene over titanium dioxide loaded on $Bi_{12}TiO_{20}$. Chin. Chem. Lett. 18, 241–243.

Lin, W.J., Xie, X.F., Wang, X., Wang, Y., Segets, D., Sun, J., 2018. Efficient adsorption and sustainable degradation of gaseous acetaldehyde and o-xylene using rGO-TiO_2 photocatalyst. Chem. Eng. J. 349, 708–718.

Liu, H.L., Ma, Y.P., Chen, J.Y., Wen, M.C., Li, G.Y., An, T.C., 2019. Highly efficient visible-light-driven photocatalytic degradation of VOCs by CO_2-assisted synthesized

mesoporous carbon confined mixed-phase TiO_2 nanocomposites derived from MOFs. Appl. Catal. B Environ. 250, 337–346.
Mei, P., Wang, H.H., Guo, H., Zhang, N., Ji, S.L., Ma, Y.P., Xu, J.Q., Li, Y., Alsulami, H., Alhodaly, M.S., Hayat, T., Sun, Y.B., 2020. The enhanced photodegradation of bisphenol A by TiO_2/C_3N_4 composites. Environ. Res. 182, 109090.
Mendez-Roman, R., Cardona-Martinez, N., 1998. Relationship between the formation of surface species and catalyst deactivation during the gas-phase photocatalytic oxidation of toluene. Catal. Today 40, 353–365.
Roso, M., Lorenzetti, A., Boaretti, C., Hrelja, D., Modesti, M., 2015. Graphene/TiO_2 based photo-catalysts on nanostructured membranes as a potential active filter media for methanol gas-phase degradation. Appl. Catal. B Environ. 176, 225–232.
Uner, D.O., Ozbek, S., 1999. The deactivation behavior of the TiO_2 used as a photo-catalyst for benzene oxidation. Stud. Surf. Sci. Catal. 126, 411–414.
Wang, D., Zhao, L.X., Ma, H.Y., Zhang, H., Guo, L.H., 2017. Quantitative analysis of reactive oxygen species photogenerated on metal oxide nanoparticles and their bacteria toxicity: the role of superoxide radicals. Environ. Sci. Technol. 51, 10137–10145.
Wang, H., Wang, B.L., Ma, S.Y., 2013. Synthesis of visible-light-driven TiO_2 yolk-shell spheres with {001} facets dominated mesoporous shells. Chin. Chem. Lett. 24, 260–263.
Wang, S.B., Ang, H.M., Tade, M.O., 2007. Volatile organic compounds in indoor environment and photocatalytic oxidation: state of the art. Environ. Int. 33, 694–705.
Wei, P., Qin, D.D., Chen, J.Y., Li, Y.X., Wen, M.C., Ji, Y.M., Li, G.Y., An, T.C., 2019. Photocatalytic ozonation mechanism of gaseous n-hexane on MOx-TiO_2-foam nickel composite (M = Cu, Mn, Ag): unveiling the role of ·OH and $\cdot O_2^-$. Environ. Sci.-Nano 6, 959–969.
Weon, S., Choi, W., 2016. TiO_2 nanotubes with open channels as deactivation-resistant photocatalyst for the degradation of volatile organic compounds. Environ. Sci. Technol. 50, 2556–2563.
Weon, S., Kim, J., Choi, W., 2018. Dual-components modified TiO_2 with Pt and fluoride as deactivation-resistant photocatalyst for the degradation of volatile organic compound. Appl. Catal. B Environ. 220, 1–8.
Xu, F., Chen, J.F., Kalytchuk, S., Chu, L., Shao, Y.R., Kong, D.X., Chu, K.H., Sit, P.H.L., Teoh, W.Y., 2017. Supported gold clusters as effective and reusable photocatalysts for the abatement of endocrine-disrupting chemicals under visible light. J. Catal. 354, 1–12.
Yao, P.Z., Liu, H.L., Wang, D.T., Chen, J.Y., Li, G.Y., An, T.C., 2018. Enhanced visible-light photocatalytic activity to volatile organic compounds degradation and deactivation resistance mechanism of titania confined inside a metal-organic framework. J. Colloid Interface Sci. 522, 174–182.
Yu, L., Wang, L., Xu, W.C., Chen, L.M., Fu, M.L., Wu, J.L., Ye, D.Q., 2018. Adsorption of VOCs on reduced graphene oxide. J. Environ. Sci. 67, 171–178.
Yue, L., Cheng, R., Ding, W.Q., Shan, J.W., Li, J., Lyu, J.Z., 2019. Composited micropores constructed by amorphous TiO_2 and graphene for degrading volatile organic compounds. Appl. Surf. Sci. 471, 1–7.
Zhang, M.L., An, T.C., Fu, J.M., Sheng, G.Y., Wang, X.M., Hu, X.H., Ding, X.J., 2006. Photocatalytic degradation of mixed gaseous carbonyl compounds at low level on adsorptive TiO_2/SiO_2 photocatalyst using a fluidized bed reactor. Chemosphere 64, 423–431.
Zhang, Q., Zheng, Y.X., Tong, D., Shao, M., Wang, S.X., Zhang, Y.H., Xu, X.D., Wang, J. N., He, H., Liu, W.Q., Lei, Y., Li, J.H., Wang, Z.F., Zhang, X.Y., Wang, Y.S., Cheng, J., Liu, Y., Shi, Q.R., Yan, L., Geng, G.N., Hong, C.P., Li, M., Liu, F., Zheng, B., Cao, J.J., Ding, A.J., Gao, J., Fu, Q.Y., Huo, J.T., Liu, B.X., Liu, Z.R., Yang, F.M., He, K.B., Hao, J.M., 2019a. Drivers of improved PM2.5 air quality in China from 2013 to 2017. P. Natl. Acad. Sci. USA 116, 24463–24469 org/10.1073/pnas.1907956116.
Zhang, W.P., Li, G.Y., Liu, H.L., Chen, J.Y., Ma, S.T., An, T.C., 2019b. Micro/nano-bubble assisted synthesis of Au/TiO_2@CNTs composite photocatalyst for photocatalytic degradation of gaseous styrene and its enhanced catalytic mechanism. Environ. Sci.-Nano 6, 948–958.
Zhang, X.Y., Gao, B., Creamer, A.E., Cao, C.C., Li, Y.C., 2017. Adsorption of VOCs onto engineered carbon materials: a review. J. Hazard Mater. 338, 102–123.
Zhang, Y.H., Tang, Z.R., Fu, X.Z., Xu, Y.J., 2010. TiO_2-graphene nanocomposites for gas-phase photocatalytic degradation of volatile aromatic pollutant: is TiO_2-graphene truly different from other TiO_2-carbon composite materials? ACS Nano 4, 7303–7314.